E 241 Survey Paper: A summary of empirical and analytical studies of resist reflow in the literature

Charmaine Chia, Joel Martis

Dating back to the ’80s, there have been numerous mentions of photoresist reflow being used in device fabrication. Surprisingly, reports of systematic empirical characterizations or analytical modelling of the reflow process have been relatively scarce. In this article, we summarize the main findings in the literature leading up to our own study, directly quoting published figures to capture the most information. In planning our splits, we aimed to generate data that would complement what has already been studied.

Since the major driving force in the reflow process is surface energy minimization, and gravitational effects are negligible, Ref 1, 2 & 4 conceptualize the ‘‘ideal’ post-reflow shape as being either a cylindrical cap (for a rectangular resist island) or spherical cap (for a circular resist island). The volume of the reflowed structure is assumed to equal the initial volume of the photoresist island, multiplied by a factor, E, to account for volume reduction. The initial and final widths of the structures are taken to be the same.

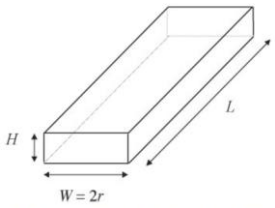

Fig. 4. The geometry of the photoresist island prior to melting, typically $L \gg W \gg H$.

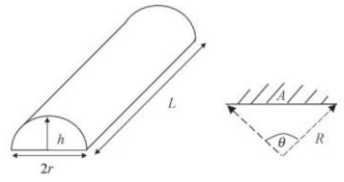

Fig. 5. Geometry of the cylindrical lens after the photoresist has melted.

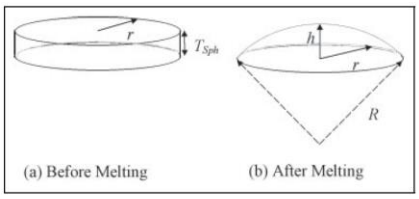

Fig. 7. The variables describing the production of spherical microlenses.

Thus, given a final width and radius of curvature R, the height of the photoresist required can be pre-determined. This model assumes the critical contact angle between the resist and substrate has no effect, and provides a starting point for approximating reflowed resist shape. Ref 2 treats critical angle as a secondary constraint, and found that for the S1818 photoresist, its dependence on reflow temperature (between 120 and 170 C) is roughly *y = -0.2431x + 48.344*. Ref 3 (a companion paper) examines 3 analytical models for describing resist shape. Model A uses a 4th order polynomial model proposed by Sheridan et al.; this is compared against Model B, a “sum model” and Model C, a “product” model, both of which use a 4th order polynomial to capture the *deviation* from the spherical idea. Coefficients are calculated using boundary conditions that include: Area, Central height, Edge=0 and Critical angle.

Ref 4 measures various geometrical properties of reflowed resist of different initial circular diameters and thicknesses of 21.4 um and 27.5 um. Unfortunately, the reflow parameters were not given. Final contact angle and radius of curvature were compared against theoretical values based on the spherical approximation, and found to deviate the most for large resist diameters.

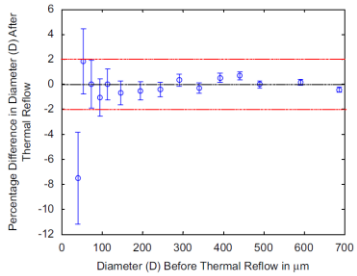

Fig. 13. Microlens diameter (D) comparison before and after reflow by optical microscope measurements with error estimation.

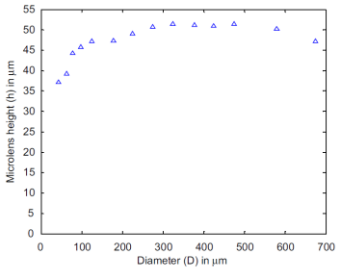

Fig. 14. Microlens height (h) measured at different values of D using contact profilometry ($t = 27.5$ µm).

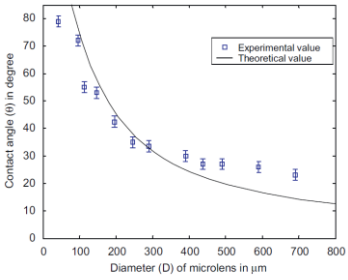

Fig. 15. Experimental plot for diameter vs. contact angle using SEM ($t = 21.4$ µm).

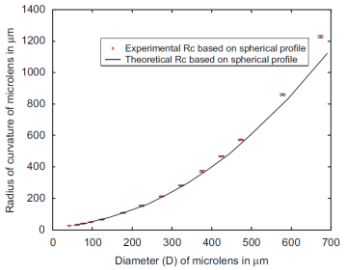

Fig. 16. Radius of curvature based on spherical profile by contact profilometer measurements ($t = 27.5$ µm).

Ref 8 investigates the main cause of deviation from the spherical model: the edge bulge effect. The position of the bulge maxima from the edge is described by d_{max}, which was empirically found to increase with reflow temperature T (propagating inwards) as: $d_{max} = h_0 \times \left((T - T_g)/T_p\right)^{1/3}$, where T_p ~ 26.6 x 10^{-3} K is a propagation constant, and T_g ~ 352.2 K is the glass temperature for SPR 220-7, obtained by fitting the data. d_{max} also increases with initial thickness h_0 until it reaches the maximum possible value of $D/2$, forming a spherical profile. As such, for a given T and width D, there is a minimum initial thickness h_0 needed to form a spherical profile after reflow.

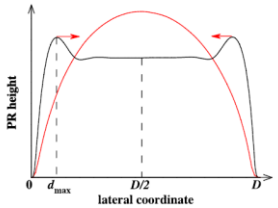

Fig. 1. (Color online) Schematic of the edge bulge effect: the curve with arrows represents a profile with an edge bulge and illustrates the key parameters d_{max} and D. The spherical curve represents the profile of a convex lens.

Ref 6 characterizes reflowed feature dimensions of rectangular AZ 50XT islands for use in microfluidics valve fabrication, focusing on the effect of initial dimensions. Reflow was done by ramping from 65 to 190 C at 10 C/h, remaining at 190 C for 4 h. The measurements establish that tall and narrow channels (with a large vertical aspect ratio) decrease in height after baking, while low and wide channels (with a small cross-sectional aspect ratio) increase in height. The pre- to post-bake height ratio (z = h/H) was fitted as a function of both the pre-bake vertical aspect ratio (x = h/w) and the pre-bake planar aspect ratio (y = l/w). This last representation can be well fitted by the following polynomial: $z = A + Bx + Cy + Dx^2 + Exy$, where the coefficients are: A =

0.630, b = 0.175, C = 0.052, D = 0.742 and E = -0.048. This can be rewritten a easily quadratic equation with the pre-bake height (h) given as a function of the desired rounded height (H), pre-bake width (w) and length (l): $\frac{DH}{w^2}h^2 + \left(\frac{EHl}{w^2} + \frac{BH}{w} - 1\right)h + H\left(A + \frac{Cl}{w}\right) = 0$, where the coefficients A to E have the same values. Solving this will provide a good approximation to the required pre-bake height needed to achieve a desired post-bake height. However, as this a purely empirical model, it remains to be seen how well the model can predict post-bake changes in height for features with drastically different dimensions. Fig 4 shows the dependence of height ratio to pre-bake vertical (A) and planar (B) aspect ratio for all the measured samples.

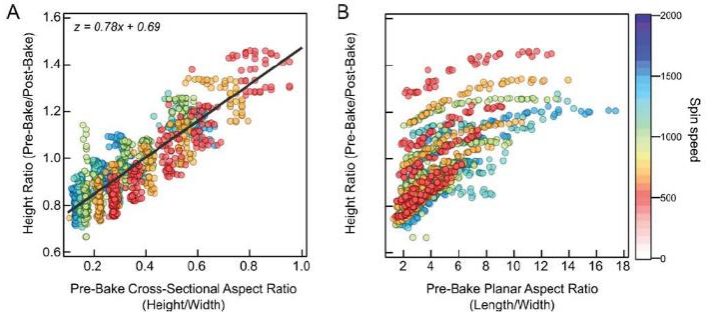

Fig. 4 Model of post-bake feature heights as a function of pre-bake aspect ratios. (A) Height ratio (pre-bake height/post-bake height) as a function of the pre-bake cross-sectional aspect ratio (measured height/width). The black line corresponds to the fit to the data shown on the figure. (B) Height ratio (pre-bake height/post-bake height) as a function of the pre-bake planar aspect ratio (measured length/width). The color of each point reflects the spin speed of the wafer.

Ref 7 adapts the energy-based, finite-element, open-source software, Surface Evolver (SE), to predict resist geometry as a function of reflow time, temperature and molecular weight. This was done by identifying two different contributions to reflow: 1) shape evolution, originating from the polymer surface tension and locally different curvatures, and 2) contact-angle evolution, driven by the polymer surface tension and the substrate surface energy. SE can calculate shape evolution based on (1), with quasi-pinning resulting from a pre-defined contact angle. To incorporate the effect of (2), a contact angle evolution time constant was calculated from direct measurement off of electron micrographs, and used to predict the contact angle to input into SE. The dependence at 110 C and 120 C can be seen in Fig. 5 & 6. Thus, the developed model allows the simulation of intermediate geometries during the reflow process, and is independent from the explicit knowledge of material-specific parameters such as viscosity or glass transition temperature. Good agreement was obtained between model and experiment.

Fig. 5: Evolution of apparent contact angle at 110 C, which is below Tg of the low molecular weight PMMA

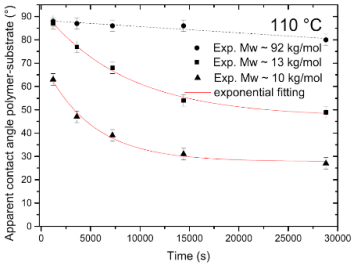

Fig. 6: Evolution of apparent contact angle at 120 C, which is well above Tg of the all the weights

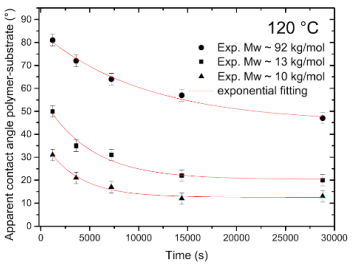

Fig 7: Experimental and simulated resist profiles as a function of time, at 120 C

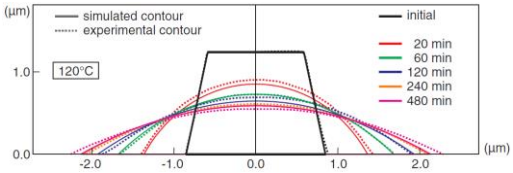

Ref 5 shows how to achieve enhanced control over final reflowed resist dimensions by studying the effect of surface treatment. Circular SPR 220-7 resist islands of 100 um diameter were patterned on substrates treated to be either hydrophobic or hydrophilic. They were then relow baked for 5 minutes at various temperatures. With the hydrophobic substrates, a threshold *shrinkage* temperature of 140 C was observed, above which the diameter of microlenses can be then reduced down to 40% compared with the initial pattern. On hydrophilic substrates, they observed a perfect linear dependency (1.4 um/C) of microlens diameter spreading up to 70% more than the initial diameter inside a temperature reflow window of 110–140 C. For both approaches, above a *freezing* temperature of 170 C, the microlens profile characteristics are temperature independent.

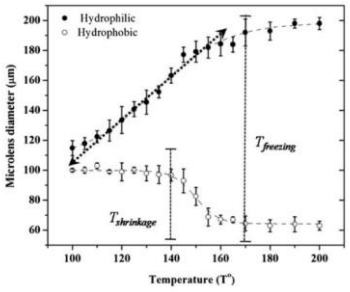

Fig. 4. Modulation of the diameter of the photoresist microlenses under the influence of chemically functionalized surface and reflow temperature (all experiments have been done with a reflow period of 5 min)–(circular pattern on the photomask is equal to 100 μm) (a) hydrophilic approach with remaining photoresist layer (filled circles), (b) Si substrate made hydrophobic by fluorosilane treatment prior photoresist dispensing (opened circles).

References

1. Nussbaum P et al. Design, fabrication and testing of microlens arrays for sensors and microsystems. Pure Appl. Opt. 1997; 6:617.
2. Feidlhim et al. Photoresist reflow method of microlens production. Part I: Background and experiments. Optik 2002; 113(9):391.
3. Feidlhim et al. Photoresist reflow method of microlens production. Part II: Analytic models. Optik 2002; 113(9):405
4. Ashraf M et al. Geometrical characterization techniques for microlens made by thermal reflow of photoresist cylinder. Optics & Lasers in Eng. 2008; 46:711.
5. Roy E et al. Microlens array fabrication by enhanced thermal reflow process: Towards efficient collection of fluorescence light from microarrays. Microelectronic Engineering 2009; 86:2255.
6. Fordyce PM et al. Systematic characterization of feature dimensions and closing pressures for microfluidic valves produced via photoresist reflow. Lab on a Chip 2012; 12:4287.
7. Kirchner R et al. Energy-based thermal reflow simulation for 3D polymer shape prediction using Surface Evolver. J. Micromech. Microeng. 2014; 24:055010.
8. Liu H et al. Control of edge bulge evolution during photoresist reflow and its application to diamond microlens fabrication. J. Vac. Sci. Technol. B 2016; 34(2): 021602